

---

# Local-peak scale-invariant feature transform for fast and random image stitching

Hao Li<sup>1</sup>, Lipo Wang<sup>2</sup>, Tianyun Zhao<sup>3</sup>, Wei Zhao<sup>1,\*</sup>

1. State Key Laboratory of Photon-Technology in Western China Energy, International Collaborative Center on Photoelectric Technology and Nano Functional Materials, Institute of Photonics & Photon Technology, Northwest University, Xi'an 710127, China
  2. UM-SJTU Joint Institute, Shanghai Jiao Tong University, Shanghai 200030, China
  3. School of Automation, Northwestern Polytechnical University, Xi'an 710072, China
- Correspondence: zwbayern@nwu.edu.cn

## Abstract

Image stitching aims to construct a wide field of view with high spatial resolution, which cannot be achieved in a single exposure. Typically, conventional image stitching techniques, other than deep learning, require complex computation and thus computational pricy, especially for stitching large raw images. In this study, inspired by the multiscale feature of fluid turbulence, we developed a fast feature point detection algorithm named local-peak scale-invariant feature transform (LP-SIFT), based on the multiscale local peaks and scale-invariant feature transform method. By combining LP-SIFT and RANSAC in image stitching, the stitching speed can be improved by orders, compared with the original SIFT method. Nine large images (over 2600×1600 pixels), arranged randomly without prior knowledge, can be stitched within 158.94 s. The algorithm is highly practical for applications requiring a wide field of view in diverse application scenes, e.g., terrain mapping, biological analysis, and even criminal investigation.

Keywords: image stitching, LP-SIFT, image mosaic

## 1. Introduction

Image stitching is employed to reconstruct complete image information from its fragments [1]. Due to the limited capability to capture a large area with high spatial resolution, image stitching finds widespread uses in engineering applications such as machine vision [2-5], augmented reality [6-9], navigation [10, 11] and panoramic shooting [12-14] etc. Furthermore, it plays an indispensable role in supporting scientific research, such as the construction of large-scale bioimages [15-19], micro/nanostructures [20-22], aerial photography [23-25] and space remote sensing [26] etc.

Various image stitching techniques can be traced back to the late 1970s or early 1980s [27-29] aiming to merge multiple images to achieve a wider field of view. In that early stages,

multiple images of the same scene were simply superimposed [30]. To now, advanced image stitching techniques can be primarily categorized into two categories: region-based and feature-based [28]. In comparison to the computationally intensive region-based stitching techniques [13], feature-based techniques impose fewer requirements on region overlapping [31], rendering them increasingly appealing in recent years. Harris et al. [32] initially proposed a feature-based stitching technique for detecting features in images based on corner points. Subsequently, Lowe et al. [33] introduced the scale-invariant Feature Transform (SIFT) approach for feature detection, utilizing the Gaussian pyramid and Gaussian difference pyramid. Although SIFT has a series of features, such as robustness, scale invariance and rotation invariance, it necessitates substantial computational resources, leading to a slower

---

feature point detection, and accordingly, lower stitching speed.

To address the limitations of SIFT, Rosten et al. [34] proposed the Features from Accelerated Segment Test (FAST), a machine learning algorithm for high-speed corner detection. However, FAST sacrifices scale invariance and rotation invariance features. To mitigate these drawbacks, Bay et al. [35] proposed the Speeded Up Robust Features (SURF) algorithm in 2008, which introduced a new scale and rotation invariant detector and descriptor. While SURF offers scale invariance, and rotation invariance, it is less robust to viewpoint changes. In 2011, Rublee et al. [36] presented an efficient alternative to SIFT and SURF, named as Oriented FAST and Rotated BRIEF (ORB). However, it is susceptible to variations in illumination.

Although in recent years, the research focuses are shifting more toward the deep-learning neural network [37-39], it is still effective to optimize and update the conventional algorithms for image stitching applications. For instance, the parity algorithm by Wu et al. [40], as an improvement of SIFT, can reduce the matching error with better accuracy. The segmentation algorithm by Gan et al. [41] helps to improve the stitching speed and the SIFT accuracy. An image registration method [42] combines Shi-Tomasi with SIFT to improve the matching accuracy and reduce the computational cost.

In feature-based image stitching techniques, the precise definition and detection of feature points are pivotal. The algorithm's efficiency can be significantly enhanced if there is a reasonable replacement for the Gaussian pyramid and Gaussian difference pyramid operations in SIFT. In the Dissipation Element (DE) analyses of

turbulent flows [43, 44], the dynamic nature of the field can be characterized by the statistics of the statistical properties of the extremal points. Moreover, the concept of extremal points can be extended to the multiscale level [45]. From a geometric standpoint, any image can be viewed as a structure with multiscale intensity, akin to the identified DEs.

In this study, we aim to construct a fast feature point detection algorithm, termed Local-Peak Scale-Invariant Feature Transform (LP-SIFT), which integrates SIFT with the concept of local extremal points or image peaks at the multiscale level. Specifically, the featured points can be substituted with the multiscale local peak points without reliance on the Gaussian pyramid and differential pyramid in SIFT. Consequently, the efficiency of feature point detection can be significantly enhanced. Additionally, by combining LP-SIFT and RANSAC in image stitching, the stitching speed can be notably improved, particularly in the processing of large images. Finally, we demonstrate that random images or segments of a large image can be successfully stitched within an acceptable time without requirement of prior knowledge.

## 2. Materials and methods

The principle of the LP-SIFT method is schematically diagramed in Fig. 1. Generally, there are five sub steps, including image preprocessing, feature point detection, feature point description, feature point matching and image stitching. We will initially provide a detailed introduction to each step. Subsequently, a strategy of applying LP-SIFT to restore a large image from random image fragments will be elucidated.

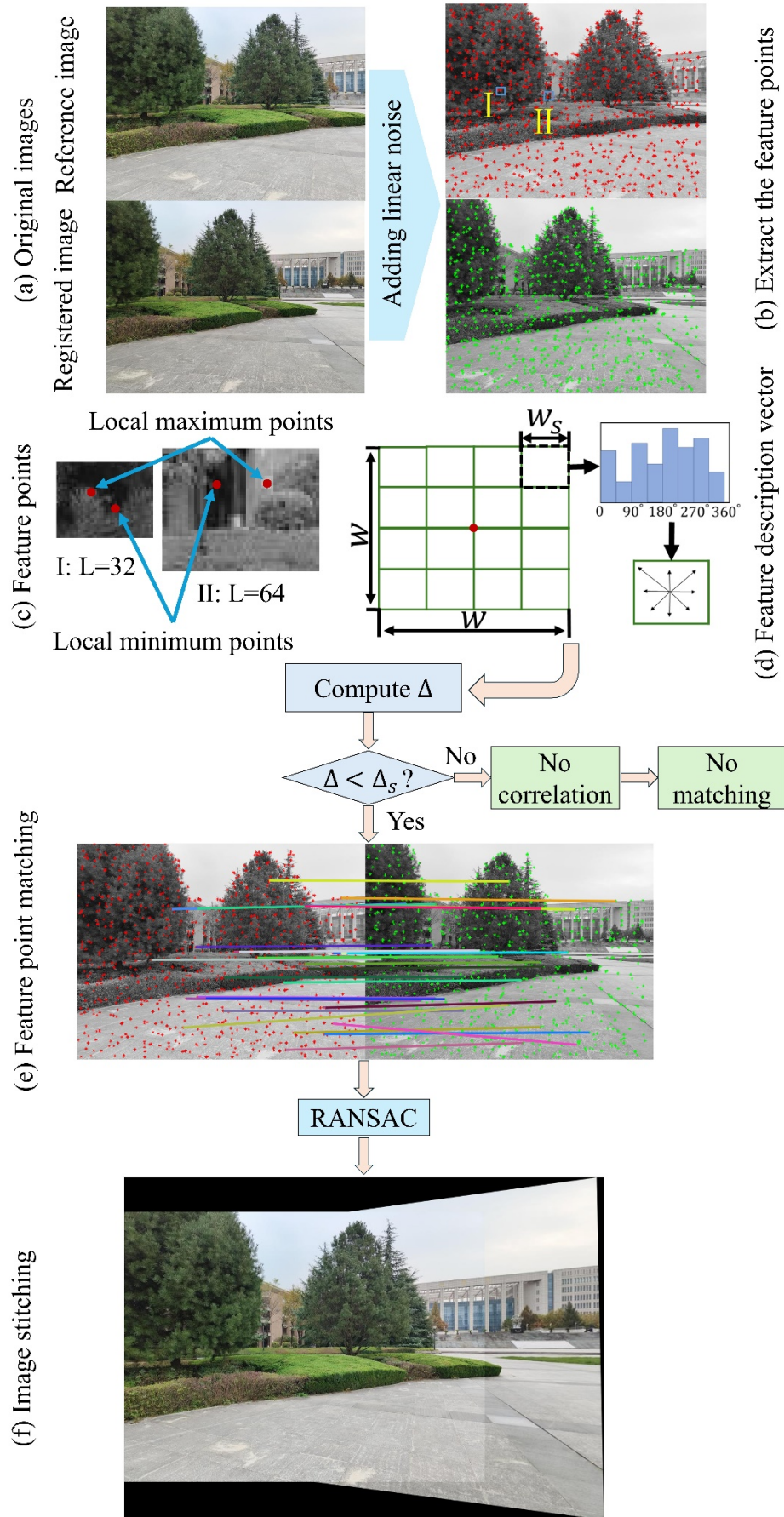


Figure 1. Diagram of the LP-SIFT method.

## 2.1 Image preprocessing

In the following exemplified case, the two images (Fig. 1(a)) designated for stitching are referred to as the reference image (stored as the reference matrix  $M_1$ ) and registered image (stored as the registration matrix  $M_2$ ), respectively. Since the feature points adopted in LP-SIFT are the local peak points (both maximum and minimum), to avoid the difficulty to locate them in the constant image intensity region, e.g. due to saturation, it is numerically meaningful to first impose a small linear background to both images. Therefore, the new image matrixes  $M_{n,k}$  becomes

$$M_{n,k}(i,j) = M_k(i,j) + [(i-1) * nc_k + j] * \alpha, \quad (1)$$

where  $\alpha \ll 1$  is the linear noise coefficient. Now the size of  $M_{n,k}$  is  $nr_k \times nc_k$ , where  $k=1$  represents parameters of the reference image and  $k=2$  represents parameters of the registered image.

## 2.2 Feature point detection

In step 2, we utilize the local peak points of multiscale images as the feature points (Fig. 1(b)). Both the reference image and the registered image are partitioned into squared interrogation windows of size  $L$ , with varying scales, e.g.  $L=32$  to  $128$ . The maximum and minimum points in each interrogation window are collected as feature points, which can be formulated as

$$\begin{cases} M_{n,k,max}(p,L) = \max[M_{np,k}(i,j)], i,j \in [0,L] \\ M_{n,k,min}(p,L) = \min[M_{np,k}(i,j)], i,j \in [0,L] \end{cases} \quad (2)$$

where  $M_{np,k}(i,j)$  is the  $p$ th interrogation window of  $L \times L$  pixels.

## 2.3 Feature point description

Once all the feature points are gathered, the SIFT feature description vector is employed to characterize the acquired feature points. First, as shown in Fig. 1(d), around each feature point (represented by red spot), a square region with the size  $w$  is extracted, with

$$w = \beta Ld, \quad (3)$$

where  $\beta = \beta_0(L/L_{max})^{-1/2}$  is an adjustable factor to control the size of the square region and  $\beta_0$  is the initial  $\beta$  when the interrogation window size  $L$  equals to its maximum value  $L_{max}$  (e.g. 128). To ensure  $w$  is not over  $L$ , it requires

$$\beta_0 \leq \frac{1}{d} \left( \frac{L}{L_{max}} \right)^{-\frac{1}{2}}. \quad (4)$$

We further divide the square region into  $d \times d$  subregions, e.g.  $d=4$  as commonly used [46]. In each subregion  $M_{n,k,s}$ , there are  $w_s \times w_s$  pixels, with  $w_s = \beta L$  as the side length of the subregion. At each pixel  $(i,j)$  in this subregion, the magnitude  $f_k(i,j)$  and orientation  $\theta_k(i,j)$  of the image gradient can be calculated as

$$\begin{cases} f_k(i,j) = \sqrt{a^2 + b^2} \\ \theta_k(i,j) = b/a \\ a = M_{n,k,s}(i+1,j) - M_{n,k,s}(i-1,j) \\ b = M_{n,k,s}(i,j+1) - M_{n,k,s}(i,j-1). \end{cases} \quad (5)$$

Then, the distribution of the image gradient in 8 directions [46] can be determined based on  $\theta_k(i,j)$  and  $f_k(i,j)$ . After the calculation along eight directions for each subregion, a 128-element array can be obtained, i.e.  $d \times d \times 8$  when  $d=4$ . Such a 128-element array is then used as the feature description vector ( $\vec{d}_f$ ) of the feature points [33]. Due to the statistical determination of the array over a wide area, the matching robustness is maintained.

## 2.4 Feature point matching

The position information (i.e. the pixel coordinates of the feature points) and feature description vector of each feature point in the reference images are denoted as  $\vec{p}_{v1}$  and  $\vec{d}_{f1}$ , respectively. The corresponding ones in registered image are denoted as  $\vec{p}_{v2}$  and  $\vec{d}_{f2}$ .

Then, the difference ( $\Delta$ ) between the feature description vectors is

$$\Delta = \sqrt{|\vec{d}_{f1} - \vec{d}_{f2}|^2}. \quad (6)$$

The smaller the difference ( $\Delta$ ) between the two feature description vectors, the more similar they are. The preset threshold of  $\Delta$  is denoted as  $\Delta_s$ . Clearly,  $\Delta_s$  signifies the requirement for similarity between the feature description vectors, thereby determining the number of matching points to be retained. Only when  $\Delta < \Delta_s$ , the  $\vec{p}_{v1}$ ,  $\vec{p}_{v2}$ ,  $\vec{d}_{f1}$  and  $\vec{d}_{f2}$  of the matched pairs are stored for image stitching.

### 2.5 Image stitching

Based on the matched pairs obtained previously, the imaging stitching process utilizes the Random Sample Consensus (RANSAC) algorithm [47]. RANSAC operates under the fundamental assumption that the sample comprises both accurate data (inliers, data that conform to the model) and abnormal data (outliers, data that deviate from the expected range and do not align with the model), which may, for instance, result from noise [48] and improper measurements, assumptions or calculations. Furthermore, RANSAC also assumes that for a given accurate dataset, the model parameters can be consistently computed.

As shown in Fig. 1(f), a homography matrix ( $H$ ) is employed to depict the perspective transformation of a plane in the real world along with its corresponding image. This matrix is utilized to facilitate the transformation of the image from one viewpoint to another through the perspective transformation process. Therefore, the relationship between the matched pairs can be obtained as follows

$$\begin{bmatrix} x' \\ y' \\ 1 \end{bmatrix} = H \begin{bmatrix} x \\ y \\ 1 \end{bmatrix} \quad (7)$$

with

$$H = \begin{bmatrix} \cos \theta & -\sin \theta & t_x \\ \sin \theta & \cos \theta & t_y \\ 0 & 0 & 1 \end{bmatrix} \quad (8)$$

where  $(x, y)$  represents the pixel coordinates of the matched points in the reference image.  $(x', y')$  represents the pixel coordinates of the matching points in the registered image. In Eq. (8),  $\theta$  represents the angular difference between the reference image and the registered image  $t_x$  and  $t_y$  represent the translational difference between the reference image and the registered image. Through the matched pairs,  $H$  can be straightforwardly determined.

### 3. Results of stitching on two images

In this section, we present a performance evaluation of the LP-SIFT algorithm, along with comparative results from other algorithms such as SIFT, ORB, and SURF. For validation purposes, the operations were conducted on a Windows 11 system equipped with an Intel Core i9-12900 processor, 64 GB memory, and an NVIDIA GeForce RTX 3090 graphics card. The LP-SIFT algorithm was implemented using MATLAB 2021a with parallel computing. To ensure consistent comparison across different scenarios, the SIFT, ORB, SURF, and LP-SIFT algorithms were utilized to compute feature points and feature description vectors in the two images. Subsequently, the RANSAC algorithm was employed to stitch the images together.

#### 3.1 Images of small size (615×820 pixels)

Small-sized images are commonly employed in various fields such as medical imaging [18], industrial inspection [49-51], and bridge inspection [52]. Hence, the performance of image stitching, which combines LP-SIFT and RANSAC, is initially assessed for these small-sized images. Fig. 2(a) and (b) depict the reference and registered images respectively.

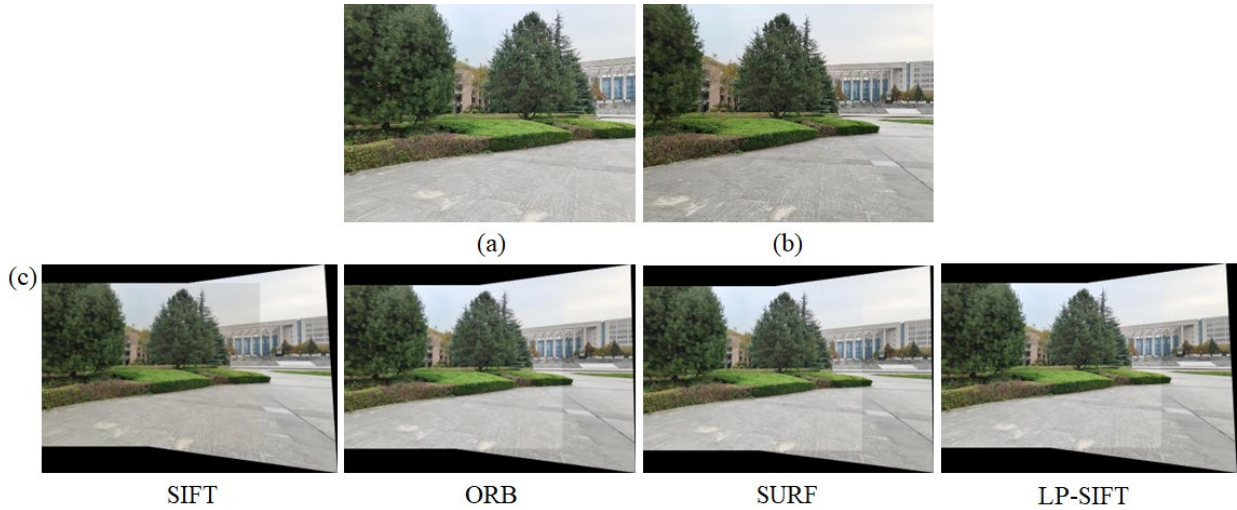


Figure 2. Reference image (a) and registered image (b) with the size of  $615 \times 820$  pixels. The stitching results of SIFT, ORB, SURF and LP-SIFT algorithms are collectively shown in (c). SIFT is from <https://github.com/haoningwu3639/ImageStitching>. ORB is from [https://blog.csdn.net/weixin\\_43764974/article/details/121743141](https://blog.csdn.net/weixin_43764974/article/details/121743141). SURF is from [https://blog.csdn.net/david\\_han008/article/details/53176145](https://blog.csdn.net/david_han008/article/details/53176145).

The stitching results are collectively shown in Fig. 2(c), incorporating those obtained using SIFT, ORB, SURF and LP-SIFT. The corresponding parameters of the stitching process are summarized in Table 2. It is evident that all four feature point detection algorithms, when combined with RANSAC can successfully stitch the two images with comparable quality. However, there are significant differences in computation times. Specifically, Fig. 3 indicates 491.37s for SIFT, 2.48s for ORB, 0.95s for SURF, and 0.79s for LP-SIFT. It should be noted that the computation time encompasses feature point detection, feature description vectors calculation, pair matching and image stitching. In summary, SIFT is the most computationally expensive, while LP-SIFT is the fastest algorithm.

### 3.2 Images of medium size ( $1080 \times 1920$ pixels)

For the purpose of high-quality visual presentation of photos [53], videos [54] and other scenes, images of 1080P ( $1080 \times 1920$  pixels) are

commonly utilized. Fig. 4(a) and (b) respectively depict the reference and registered images of the medium size.

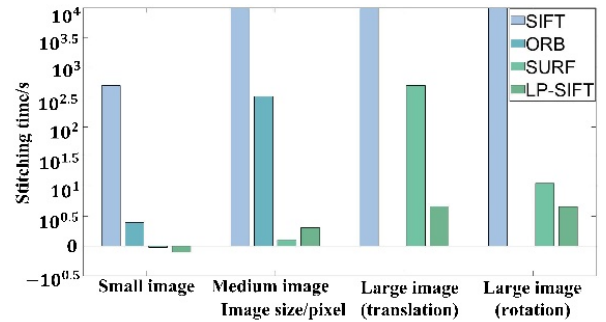


Figure 3. Comparison of the stitching times of different algorithms for different image sizes

Fig. 4(c) shows the stitching results obtained by ORB, SURF and LP-SIFT, respectively. The corresponding parameters can be found in Table 2. Again, the three feature point detection algorithms, when combined with RANSAC, can successfully stitch the two images. The differences are, ORB algorithm takes 327.25 s, SURF algorithm takes 1.28 s, and LP-SIFT algorithm takes 2.03 s. Since the SIFT algorithm

takes more than  $10^4$  s but doesn't return any matching result, we stopped the algorithm and did not test the stitching time. In this computation set, both the SURF and LP-SIFT algorithms

require significantly less time than ORB, which experiences a notable increase in the number of feature points as the image size is enlarged.

Table 2. Parameter setup of different feature point detection algorithm. To maintain the consistency for comparison, all the of them were stitched by RANSAC algorithm. SIFT is from <https://github.com/haoningwu3639/ImageStitching>. ORB is from [https://blog.csdn.net/weixin\\_43764974/article/details/121743141](https://blog.csdn.net/weixin_43764974/article/details/121743141). SURF is from [https://blog.csdn.net/david\\_han008/article/details/53176145](https://blog.csdn.net/david_han008/article/details/53176145).

Image		Algorithm	Number of feature points		Number of matched pairs	Window size ( $L$ )	Stitching time (s)
Small image	615×820	SIFT	2323	1978	23	×	491.37
		ORB	19562	15349	2215	×	2.48
		SURF	783	685	293	×	0.95
		LP-SIFT	247	230	42	[64,128]	0.79
Medium image	1080×1920	SIFT	×	×	×	×	$>10^4$
		ORB	107612	108452	9720	×	327.25
		SURF	6123	5985	1780	×	1.28
		LP-SIFT	532	484	17	[100,128]	2.03
Large image (translation)	3072×4096	SIFT	×	×	×	×	$>10^4$
		ORB	1739052	1684698	Over size	×	×
		SURF	99324	96309	30093	×	493.37
		LP-SIFT	423	435	41	[256,512]	4.62
Large image (rotation)	3072×4096	SIFT	×	×	×	×	$>10^4$
		ORB	1326389	1332929	Over size	×	×
		SURF	47568	47678	11293	×	11.42
		LP-SIFT	422	429	22	[256,512]	4.58

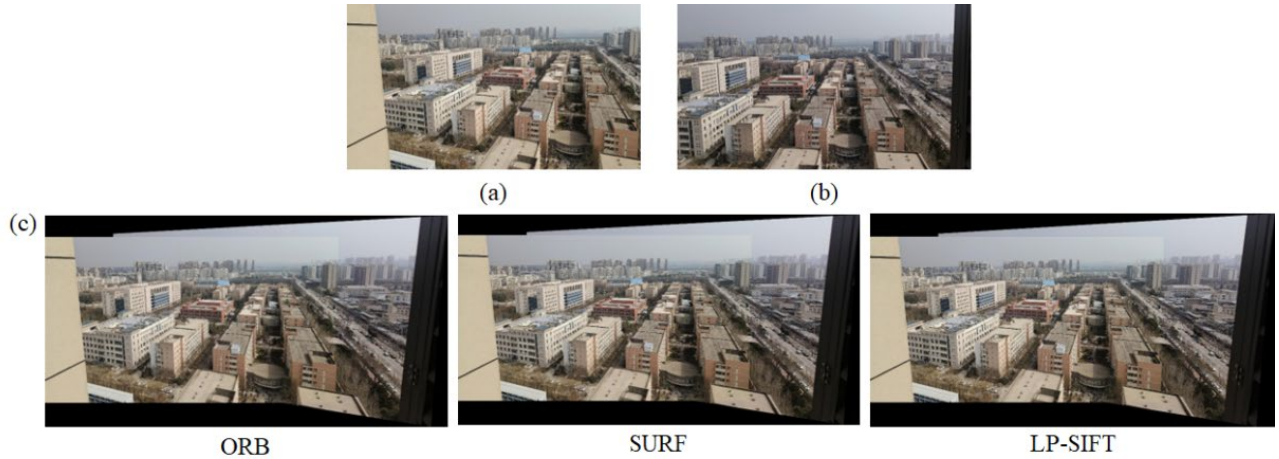


Figure 4. Original images and their stitching. (a) Reference and (b) registered images. The images size is  $1080 \times 1920$  pixels. The stitching results of ORB, SURF and LP-SIFT algorithms are shown in (c) respectively. ORB is from [https://blog.csdn.net/weixin\\_43764974/article/details/121743141](https://blog.csdn.net/weixin_43764974/article/details/121743141). SURF is from [https://blog.csdn.net/david\\_han008/article/details/53176145](https://blog.csdn.net/david_han008/article/details/53176145).

### 3.3 Images of large size ( $3072 \times 4096$ pixels) with translational displacement

Large-sized images are frequently employed in mobile photography [55, 56], satellite remote sensing [57, 58], UAV aerial photography [23, 59] and other fields. Consequently, we have chosen a collection of large-sized images to assess the performance of LP-SIFT. Fig. 5(a) and (b) depict the reference and registered images, with the same size of  $3072 \times 4096$  pixels.

Fig. 5(c) depicts the stitching results achieved by combining the SURF and LP-SIFT feature point detection algorithms with RANSAC, along with the stitching parameters summarized in Table 2. Both feature point detection algorithms successfully stitched the two images with RANSAC. However, the former takes 493.37 s, while the latter takes 4.62 s. Since the execution time for SIFT exceeded  $10^4$  s without yielding

any results, the computation was halted at that point. On the other hand, the ORB algorithm detected an excessive number of feature points, surpassing the computer's memory capacity and leading to a stitching failure. Among the four algorithms, LP-SIFT exhibits orders of improvement on stitching speed. One key advantage of LP-SIFT is its adjustable interrogation window size, allowing for the control of the number of feature points even in extremely large images with high signal-to-noise ratio (SNR). By applying a larger interrogation window size, LP-SIFT can effectively limit the number of feature points, resulting in a faster stitching process compared to other algorithms. This enhanced efficiency makes LP-SIFT a compelling choice for image stitching tasks, especially in scenarios where computational resources are limited.

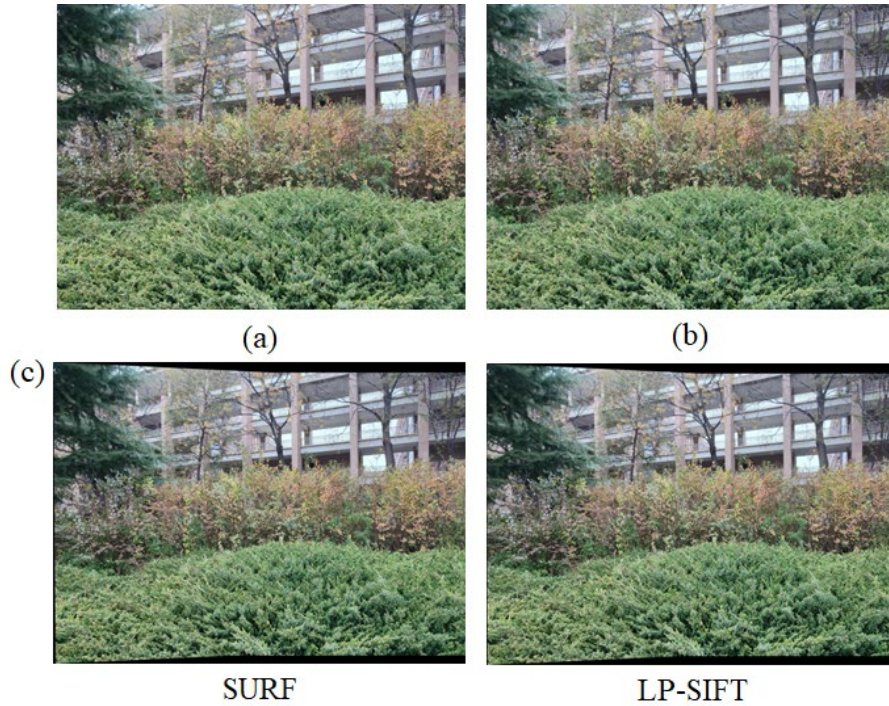


Figure 5. Original images and their stitching. (a) Reference and (b) registered images. The images size is  $3072 \times 4096$  pixels. The stitching results of SURF and LP-SIFT algorithms are shown in (c) respectively. SURF is from [https://blog.csdn.net/david\\_han008/article/details/53176145](https://blog.csdn.net/david_han008/article/details/53176145).

### 3.4 Images of large size ( $3072 \times 4096$ pixels) with rotational displacement

SIFT algorithm has rotation invariance. In this section, we hope to demonstrate LP-SIFT algorithm also reserve rotation invariance feature. Fig. 6(a) and (b) are the reference and registered images respectively, with the same size of  $3072 \times 4096$  pixels. They are captured separately by the same camera, not artificially rotated from each other. The SIFT, ORB, SURF, LP-SIFT algorithms were employed to detect feature points and feature description vectors. RANSAC algorithm is further used to stitch the images. Fig. 6(c) depicts the stitching results achieved by combining the SURF and LP-SIFT feature point detection algorithms with RANSAC, along with the stitching parameters summarized in Table 2. It is evident that both feature point detection algorithms can successfully stitch the two images with comparable quality. However, SURF

algorithm takes 11.42 s, while LP-SIFT algorithm takes 4.58 s, which is only 40% of the computation time by SURF. Similar as in section 3.3, SIFT algorithm requires an unacceptable long time for stitching, while ORB algorithm fails in stitching due to the overflow of memory. Therefore, LP-SIFT shows the capability of stitching images with rotational displacements, particularly fast for the images with large size.

### 3.5 Discussion

From the comparison of stitching images of different sizes, the performance of LP-SIFT is evaluated. Uniquely different from SIFT, ORB and SURF, LP-SIFT is flexible to adjust the interrogation window size to determine the multi-scale local peaks. Therefore, the number of feature points can be well controlled without a significant increase with the image size, which is then advantageous to replace the Gaussian

---

pyramid and difference pyramid feature point detection.

The test results demonstrate that compared to the original SIFT method, the speed of feature point detection can be improved by 622 times for small size images and by orders of magnitude for larger image cases. The time consumption in SIFT is primarily attributed to the calculation of feature description vectors, particularly when

dealing with a large number of detected feature points, especially in the case of large images. However, ORB faces challenges in real scenarios due to the rapid increase in feature points with image size. SURF algorithm is applicable for stitching images of different sizes, but the overall efficiency is relatively lower than LP-SIFT.

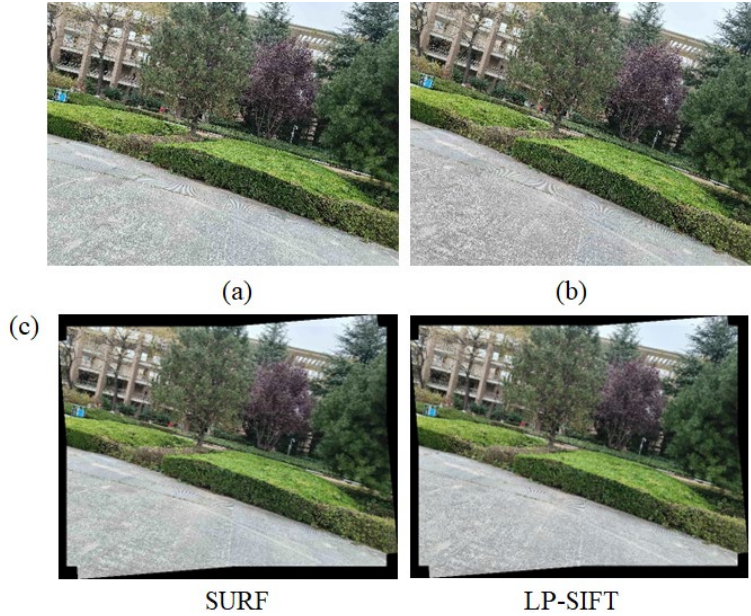


Figure 6. Original images and their stitching. (a) Reference and (b) registered images. The images size is  $3072 \times 4096$  pixels. The stitching results of SURF and LP-SIFT algorithms are shown in (c) respectively. SURF is from [https://blog.csdn.net/david\\_han008/article/details/53176145](https://blog.csdn.net/david_han008/article/details/53176145).

#### 4. Mosaic of multiple images without prior knowledge

In various application scenes, e.g. criminal investigation [60], remote sensing monitoring [58] and UAV aerial photography [59] etc., images are very probably fragmented with unknown positions, angles and sequences that need to be restored. Thus, the mosaic strategy of stitching multiple images, which is more complex than the two-image case, is also crucial. Here we propose a mosaic strategy for combining multiple images without prior knowledge.

As illustrated in Fig. 7, the first step involves using LP-SIFT to compute the homography matrix between each pair of images within a given data set, which is stored to the matrix ( $H_M$ ). This process can be parallelized using CPU computing. Subsequently, the number of nonzero elements in each row or column of  $H_M$  is counted, and the reference image is selected based on the row or column with the highest count of nonzero elements. Then, the images matched with the reference image are stitched for the first time, and the unmatched images are stored in the unmatched set. The stitching is then performed a second time until the number in the

unmatched set is 0 to finalize the stitching process.

Fig. 8(a) depicts the original image captured in this experiment. The image size is 6400×4270. Fig. 8(b) shows the fragmented images randomly divided from the original image. The approach outlined in Fig. 7 is employed to seamlessly merge the image fragments shown in Fig. 8(b). As shown in Fig. 8(c), the result is highly coincident to the original image in Fig. 8(a). The stitching time is 158.94 s, which is acceptable for a wide range of applications.

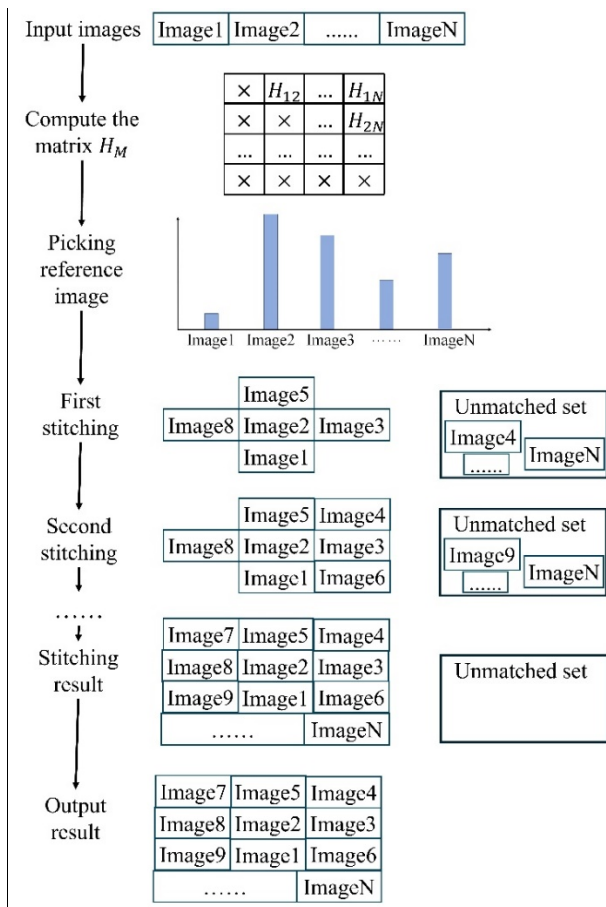


Figure 7. Schematic diagram of LP-SIFT image mosaic of multiple images without prior knowledge

## 5. Conclusions

In this study, we propose a fast feature point detection algorithm, namely Local-peak scale-

invariant feature transform (LP-SIFT), which integrates the concept of local extremal points or image peaks at the multiscale level with SIFT. By integrating LP-SIFT and RANSAC in image stitching, significant improvements in stitching speed are achieved compared to the original SIFT method. Furthermore, LP-SIFT evaluated against ORG and SURF for stitching images of varying sizes. Due to its adaptability in adjusting the interrogation window size, LP-SIFT demonstrates minimal increase in the number of detected feature points with increasing image size, resulting in noticeable reduction in stitching time particularly for large-scale cases. Additionally, we also provide a strategy for seamlessly stitching multiple images using LP-SIFT without prior knowledge. It is anticipated that LP-SIFT will contribute to diverse application scenarios such as terrain mapping, biological analysis, and even criminal investigations.

## Author Contributions:

**Hao Li:** Investigation, Visualization, Writing-Original draft preparation, Software. **Lipo Wang:** Methodology, Writing- Reviewing and Editing. **Tianyun Zhao:** Writing- Reviewing and Editing. **Wei Zhao:** Supervision, Conceptualization, Methodology, Data curation, Validation, Writing- Reviewing and Editing.

**Funding:** National Natural Science Foundation of China (51927804, 61378083, 61775181).

**Conflicts of Interest:** The authors declare no conflict of interest.

**Statement:** During the preparation of this work the author(s) used ChatGPT 3.5 in order to check essay presentation, grammar, and spelling. After using this tool, the authors reviewed and edited the content as needed and take full responsibility for the content of the publication.

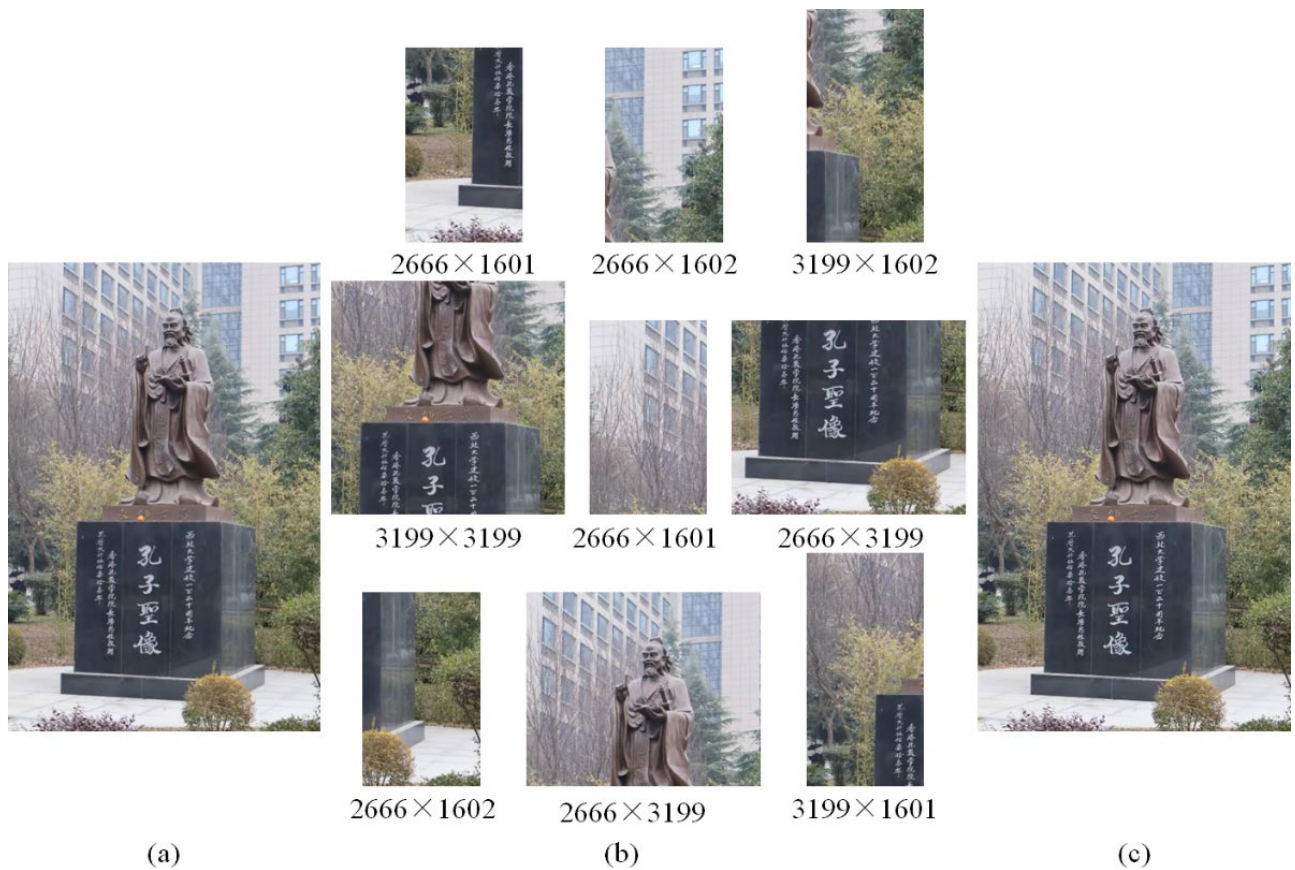


Figure 8. Mosaic of multiple images without prior knowledge. (a) Original image, the image size is 6400×4270. (b) The original image is stitched into different sizes and its position is shuffled, and its size is marked below the image. (c) stitching result, and the stitching time is 158.94 s.

## References

- [1]P. Deshmukh and P. Paikrao. A Review of Various Image Mosaicing Techniques, 2019 Innovations in Power and Advanced Computing Technologies (I-Pact), 2019. <https://doi.org/10.1109/i-pact44901.2019.8960220>.
- [2]W. T. Lee, H. I. Chen, M. S. Chen, I. C. Shen and B. Y. Chen. High - Resolution 360 Video Foveated Stitching for Real - Time Vr, Computer Graphics Forum, 2017: 115-123. <https://doi.org/10.1111/cgf.13277>.
- [3]S. Saeed, M. U. Kakli, Y. Cho, J. Seo and U. Park. A High-Quality Vr Calibration and Real-Time Stitching Framework Using Preprocessed Features, IEEE Access, 2020: 190300-190311. <https://doi.org/10.1109/access.2020.3031413>.
- [4]P. Dang, J. Zhu, Y. Zhou, Y. Rao, J. You, J. Wu, M. Zhang and W. Li. A 3d-Panoramic Fusion Flood Enhanced Visualization Method for Vr, Environmental Modelling & Software, 2023. <https://doi.org/10.1016/j.envsoft.2023.105810>.
- [5]Z. Liu and S. Chang. A Study of Digital Exhibition Visual Design Led by Digital Twin and Vr Technology, Measurement: Sensors, 2024. <https://doi.org/10.1016/j.measen.2023.100970>.
- [6]T. Greibe, T. A. Anhøj, L. S. Johansen and A. Han. Quality Control of Jeol Jbx-9500fsz E-Beam Lithography System in a Multi-User Laboratory, Microelectronic Engineering, 2016: 25-28. <https://doi.org/10.1016/j.mee.2016.02.003>.
- [7]J. Pan, W. Liu, P. Ge, F. Li, W. Shi, L. Jia and H. Qin. Real-Time Segmentation and Tracking of Excised Corneal Contour by Deep Neural Networks

---

for Dalk Surgical Navigation, *Computer Methods and Programs in Biomedicine*, 2020. <https://doi.org/10.1016/j.cmpb.2020.105679>.

[8]Y. Wang and J. Yang. Origin of Organic Matter Pore Heterogeneity in Oil Mature Triassic Chang-7 Mudstones, Ordos Basin, China, *International Journal of Coal Geology*, 2024. <https://doi.org/10.1016/j.coal.2024.104458>.

[9]Q. Zhou and Z. Zhou. Web-Based Mixed Reality Video Fusion with Remote Rendering, *Virtual Reality & Intelligent Hardware*, 2023: 188-199. <https://doi.org/10.1016/j.vrih.2022.03.005>.

[10]Z. He, Z. He, S. Li, Y. Yu and K. Liu. A Ship Navigation Risk Online Prediction Model Based on Informer Network Using Multi-Source Data, *Ocean Engineering*, 2024. <https://doi.org/10.1016/j.oceaneng.2024.117007>.

[11]B. Wang, S. Gou, K. Di, W. Wan, M. Peng, C. Zhao, Y. Zhang and B. Xie. Rock Size-Frequency Distribution Analysis at the Zhurong Landing Site Based on Navigation and Terrain Camera Images Along the Entire Traverse, *Icarus*, 2024. <https://doi.org/10.1016/j.icarus.2024.116001>.

[12]M. Cao, L. Zheng, W. Jia and X. Liu. Constructing Big Panorama from Video Sequence Based on Deep Local Feature, *Image and Vision Computing*, 2020. <https://doi.org/10.1016/j.imavis.2020.103972>.

[13]W. Lyu, Z. Zhou, L. Chen and Y. Zhou. A Survey on Image and Video Stitching, *Virtual Reality & Intelligent Hardware*, 2019: 55-83. <https://doi.org/10.3724/sp.J.2096-5796.2018.0008>.

[14]Q. Wang, F. Reimeier and K. Wolter. Efficient Image Stitching through Mobile Offloading, *Electronic Notes in Theoretical Computer Science*, 2016: 125-146. <https://doi.org/10.1016/j.entcs.2016.09.027>.

[15]R. Torres, G. Mahalingam, D. Kapner, E. T. Trautman, T. Fliss, S. Seshamani, E. Perlman, R. Young, S. Kinn, J. Buchanan, M. M. Takeno, W. Yin, D. J. Bumbarger, R. P. Gwinn, J. Nyhus, E. Lein, S. J. Smith, R. C. Reid, K. A. Khairy, S. Saalfeld, F.

Collman and N. Macarico da Costa. A Scalable and Modular Automated Pipeline for Stitching of Large Electron Microscopy Datasets, *eLife*, 2022. <https://doi.org/10.7554/eLife.76534>.

[16]B. Ma, T. Zimmermann, M. Rohde, S. Winkelbach, F. He, W. Lindenmaier and K. E. J. Dittmar. Use of Autostitch for Automatic Stitching of Microscope Images, *Micron*, 2007: 492-499. <https://doi.org/10.1016/j.micron.2006.07.027>.

[17]F. Yang, Z.-S. Deng and Q.-H. Fan. A Method for Fast Automated Microscope Image Stitching, *Micron*, 2013: 17-25. <https://doi.org/10.1016/j.micron.2013.01.006>.

[18]F. Yang, Y. He, Z. S. Deng and A. Yan. Improvement of Automated Image Stitching System for Dr X-Ray Images, *Computers in Biology and Medicine*, 2016: 108-114. <https://doi.org/10.1016/j.compbimed.2016.01.026>.

[19]J.-H. Seo, S. Yang, M.-S. Kang, N.-G. Her, D.-H. Nam, J.-H. Choi and M. H. Kim. Automated Stitching of Microscope Images of Fluorescence in Cells with Minimal Overlap, *Micron*, 2019. <https://doi.org/10.1016/j.micron.2019.102718>.

[20]Z. Lei, X. Liu, L. Zhao, L. Chen, Q. Li, T. Yuan and W. Lu. A Novel 3d Stitching Method for Wli Based Large Range Surface Topography Measurement, *Optics Communications*, 2016: 435-447. <https://doi.org/10.1016/j.optcom.2015.09.074>.

[21]P. Yang, S.-w. Ye and Y.-f. Peng. Three-Dimensional Profile Stitching Measurement for Large Aspheric Surface During Grinding Process with Sub-Micron Accuracy, *Precision Engineering*, 2017: 62-71. <https://doi.org/10.1016/j.precisioneng.2016.07.005>.

[22]W. Y. Kim, B. W. Seo, S. H. Lee, T. G. Lee, S. Kwon, W. S. Chang, S.-H. Nam, N. X. Fang, S. Kim and Y. T. Cho. Quasi-Seamless Stitching for Large-Area Micropatterned Surfaces Enabled by Fourier Spectral Analysis of Moiré Patterns, *Nature Communications*, 2023. <https://doi.org/10.1038/s41467-023-37828-8>.

- 
- [23]A. Feng, C. N. Vong, J. Zhou, L. S. Conway, J. Zhou, E. D. Vories, K. A. Sudduth and N. R. Kitchen. Developing an Image Processing Pipeline to Improve the Position Accuracy of Single Uav Images, *Computers and Electronics in Agriculture*, 2023. <https://doi.org/10.1016/j.compag.2023.107650>.
- [24]S. Feng, M. Gao, X. Jin, T. Zhao and F. Yang. Fine-Grained Damage Detection of Cement Concrete Pavement Based on Uav Remote Sensing Image Segmentation and Stitching, *Measurement*, 2024. <https://doi.org/10.1016/j.measurement.2023.113844>.
- [25]X. Wang, N. He, C. Hong, Q. Wang and M. Chen. Improved Yolox-X Based Uav Aerial Photography Object Detection Algorithm, *Image and Vision Computing*, 2023. <https://doi.org/10.1016/j.imavis.2023.104697>.
- [26]W. Zeng, Q. Deng, X. Zhao, D. Li and X. Min. A Method for Stitching Remote Sensing Images with Delaunay Triangle Feature Constraints, *Geocarto International*, 2023. <https://doi.org/10.1080/10106049.2023.2285356>.
- [27]T. Rui, Y. Hu, C. Yang, D. Wang and X. Liu. Research on Fast Natural Aerial Image Mosaic, *Computers & Electrical Engineering*, 2021. <https://doi.org/10.1016/j.compeleceng.2021.107007>.
- [28]D. Ghosh and N. Kaabouch. A Survey on Image Mosaicing Techniques, *Journal of Visual Communication and Image Representation*, 2016: 1-11. <https://doi.org/10.1016/j.jvcir.2015.10.014>.
- [29]Z. Ma and S. Liu. A Review of 3d Reconstruction Techniques in Civil Engineering and Their Applications, *Advanced Engineering Informatics*, 2018: 163-174. <https://doi.org/10.1016/j.aei.2018.05.005>.
- [30]P. Deshmukh, P. J. I. i. P. Paikrao and A. C. Technologies. A Review of Various Image Mosaicing Techniques, 2019: 1-4.
- [31]M. Z. Bonny and M. S. Uddin. Feature-Based Image Stitching Algorithms, 2016 International workshop on computational intelligence (IWCI), 2016: 198-203.
- [32]C. Harris and M. Stephens. A Combined Corner and Edge Detector, *Proceedings of the Alvey Vision Conference 1988*, 1988: 23.21-23.26. <https://doi.org/10.5244/c.2.23>.
- [33]D. G. Lowe. Distinctive Image Features from Scale-Invariant Keypoints, *International Journal of Computer Vision*, 2004: 91-110. <https://doi.org/10.1023/b:Visi.0000029664.99615.94>.
- [34]E. Rosten and T. Drummond. Machine Learning for High-Speed Corner Detection, *Computer Vision–ECCV 2006: 9th European Conference on Computer Vision*, Graz, Austria, May 7-13, 2006. Proceedings, Part I 9, 2006: 430-443.
- [35]H. Bay, A. Ess, T. Tuytelaars and L. Van Gool. Speeded-up Robust Features (Surf), *Computer Vision and Image Understanding*, 2008: 346-359. <https://doi.org/10.1016/j.cviu.2007.09.014>.
- [36]E. Rublee, V. Rabaud, K. Konolige and G. Bradski. Orb: An Efficient Alternative to Sift or Surf, 2011 International conference on computer vision, 2011: 2564-2571.
- [37]G. Li, T. Li, F. Li and C. Zhang. Nervestitcher: Corneal Confocal Microscope Images Stitching with Neural Networks, *Computers in Biology and Medicine*, 2022. <https://doi.org/10.1016/j.compbimed.2022.106303>.
- [38]F. Zhu, J. Li, B. Zhu, H. Li and G. Liu. Uav Remote Sensing Image Stitching Via Improved Vgg16 Siamese Feature Extraction Network, *Expert Systems with Applications*, 2023. <https://doi.org/10.1016/j.eswa.2023.120525>.
- [39]N. ul-Huda, H. Ahmad, A. Banjar, A. O. Alzahrani, I. Ahmad and M. S. Naeem. Image Synthesis of Apparel Stitching Defects Using Deep Convolutional Generative Adversarial Networks, *Heliyon*, 2024. <https://doi.org/10.1016/j.heliyon.2024.e26466>.
- [40]Z. Wu and H. Wu. Improved Sift Image Feature Matching Algorithm, 2022 2nd International Conference on Computer Graphics, Image and Virtualization (ICCGIV), 2022: 223-226. <https://doi.org/10.1109/iccgiv57403.2022.00051>.

- 
- [41]W. Gan, Z. Wu, M. Wang and X. Cui. Image Stitching Based on Optimized Sift Algorithm, 2023 5th International Conference on Intelligent Control, Measurement and Signal Processing (ICMSP), 2023: 1099-1102.  
<https://doi.org/10.1109/icmsp58539.2023.10170989>.
- [42]X. Li and S. Li. Image Registration Algorithm Based on Improved Sift, 2023 4th International Conference on Electronic Communication and Artificial Intelligence (ICECAI), 2023: 264-267.  
<https://doi.org/10.1109/icecai58670.2023.10176776>.
- [43]L. Wang and N. Peters. The Length-Scale Distribution Function of the Distance between Extremal Points in Passive Scalar Turbulence, *Journal of Fluid Mechanics*, 2006.  
<https://doi.org/10.1017/s0022112006009128>.
- [44]N. Peters and L. Wang. Dissipation Element Analysis of Scalar Fields in Turbulence, *Comptes Rendus Mécanique*, 2006: 493-506.  
<https://doi.org/10.1016/j.crme.2006.07.006>.
- [45]L. P. Wang and Y. X. Huang. Multi-Level Segment Analysis: Definition and Application in Turbulent Systems, *Journal of Statistical Mechanics: Theory and Experiment*, 2015.  
<https://doi.org/10.1088/1742-5468/2015/06/p06018>.
- [46]D. G. Lowe. Object Recognition from Local Scale-Invariant Features, *Proceedings of the seventh IEEE international conference on computer vision*, 1999: 1150-1157.
- [47]Y. Zhang and Y. Xie. Adaptive Clustering Feature Matching Algorithm Based on Sift and Ransac, 2021 2nd International Conference on Electronics, Communications and Information Technology (CECIT), 2021: 174-179.
- [48]M. A. Fischler and R. C. J. C. o. t. A. Bolles. Random Sample Consensus: A Paradigm for Model Fitting with Applications to Image Analysis and Automated Cartography, 1981: 381-395.
- [49]D. Zhang, W. Jackson, G. Dobie, G. West and C. MacLeod. Structure-from-Motion Based Image Unwrapping and Stitching for Small Bore Pipe Inspections, *Computers in Industry*, 2022.  
<https://doi.org/10.1016/j.compind.2022.103664>.
- [50]S. Chatterjee and K. K. Issac. Viewpoint Planning and 3d Image Stitching Algorithms for Inspection of Panels, *NDT & E International*, 2023.  
<https://doi.org/10.1016/j.ndteint.2023.102837>.
- [51]S. Popovych, T. Macrina, N. Kemnitz, M. Castro, B. Nehoran, Z. Jia, J. A. Bae, E. Mitchell, S. Mu, E. T. Trautman, S. Saalfeld, K. Li and H. S. Seung. Petascale Pipeline for Precise Alignment of Images from Serial Section Electron Microscopy, *Nature Communications*, 2024.  
<https://doi.org/10.1038/s41467-023-44354-0>.
- [52]R. Xie, J. Yao, K. Liu, X. Lu, Y. Liu, M. Xia and Q. Zeng. Automatic Multi-Image Stitching for Concrete Bridge Inspection by Combining Point and Line Features, *Automation in Construction*, 2018: 265-280. <https://doi.org/10.1016/j.autcon.2018.02.021>.
- [53]W. Zhu, L. Liu, G. Jiang, S. Yin, S. J. I. T. o. C. Wei and S. f. V. Technology. A 135-Frames/S 1080p 87.5-Mw Binary-Descriptor-Based Image Feature Extraction Accelerator, 2015: 1532-1543.
- [54]X. Zhang, H. Sun, S. Chen, N. J. I. T. o. C. Zheng and S. f. V. Technology. Vlsi Architecture Exploration of Guided Image Filtering for 1080p@ 60hz Video Processing, 2016: 230-241.
- [55]M. Bordallo-Lopez, O. Silvén, M. Tico and M. Vehviläinen. Creating Panoramas on Mobile Phones, *Computational imaging V*, 2007: 54-63.
- [56]Y. Xiong and K. J. I. T. o. C. E. Pulli. Fast Panorama Stitching for High-Quality Panoramic Images on Mobile Phones, 2010: 298-306.
- [57]L. Wang, Y. Zhang, T. Wang, Y. Zhang, Z. Zhang, Y. Yu and L. J. R. S. Li. Stitching and Geometric Modeling Approach Based on Multi-Slice Satellite Images, 2021: 4663.
- [58]B. Huang, L. M. Collins, K. Bradbury and J. M. Malof. Deep Convolutional Segmentation of Remote Sensing Imagery: A Simple and Efficient Alternative to Stitching Output Labels, *IGARSS 2018-2018 IEEE International Geoscience and Remote Sensing Symposium*, 2018: 6899-6902.

---

[59]M. Ren, J. Li, L. Song, H. Li and T. Xu. Mlp-Based Efficient Stitching Method for Uav Images, IEEE Geoscience and Remote Sensing Letters, 2022: 1-5. <https://doi.org/10.1109/lgrs.2022.3141890>.

[60]G. Sansoni, M. Trebeschi and F. J. S. Docchio. State-of-the-Art and Applications of 3d Imaging Sensors in Industry, Cultural Heritage, Medicine, and Criminal Investigation, 2009: 568-601.